Common Electronic Features and Electronic Nematicity in Parent Compounds of Iron-Based Superconductors and FeSe/$SrTiO_3$ Films Revealed by Angle-Resolved Photoemission Spectroscopy *

De-Fa Liu(刘德发)[1], Lin Zhao(赵林)[1], Shao-Long He(何少龙)[1], Yong Hu(胡勇)[1], Bing Shen(沈兵)[1], Jian-Wei Huang(黄建伟)[1], Ai-Ji Liang(梁爱基)[1], Yu Xu(徐煜)[1], Xu Liu(刘旭)[1], Jun-Feng He(何俊峰)[1], Dai-Xiang Mou(牟代翔)[1], Shan-Yu Liu(刘单于)[1], Hai-Yun Liu(刘海云)[1], Guo-Dong Liu(刘国东)[1], Wen-Hao Zhang(张文号)[2], Fang-Sen Li(李坊森)[2], Xu-Cun Ma(马旭村)[2], Qi-Kun Xue(薛其坤)[2], Xian-Hui Chen(陈仙辉)[3], Gen-Fu Chen(陈根富)[1], Li Yu(俞理)[1], Jun Zhang(张君)[1], Zu-Yan Xu(许祖彦)[4], Chuang-Tian Chen(陈创天)[4], Xing-Jiang Zhou(周兴江)[1,5]**

[1]*National Laboratory for Superconductivity, Beijing National Laboratory for Condensed Matter Physics, Institute of Physics, Chinese Academy of Sciences, Beijing 100190*

[2]*State Key Lab of Low-Dimensional Quantum Physics, Department of Physics, Tsinghua University, Beijing 100084*

[3]*Hefei National Laboratory for Physical Sciences at Microscale and Department of Physics, University of Science and Technology of China, Hefei 230026*

[4]*Technical Institute of Physics and Chemistry, Chinese Academy of Sciences, Beijing 100190*

[5]*Collaborative Innovation Center of Quantum Matter, Beijing 100871*

(Received 25 May 2016)

We report comprehensive angle-resolved photoemission investigations on the electronic structures and nematicity of the parent compounds of the iron-based superconductors including CeFeAsO, $BaFe_2As_2$, NaFeAs, FeSe and undoped FeSe/$SrTiO_3$ films with 1, 2 and 20 layers. While the electronic structure near the Brillouin zone center Γ varies dramatically among different materials, the electronic structure near the Brillouin zone corners (M points), as well as their temperature dependence, are rather similar. The electronic structure near the zone corners is dominated by the electronic nematicity that gives rise to a band splitting of the d_{xz} and d_{yz} bands below the nematic transition temperature. A clear relation is observed between the band splitting magnitude and the onset temperature of nematicity. Our results may shed light on the origin of nematicity, its effect on the electronic structures, and its relation with superconductivity in the iron-based superconductors.

PACS: 74.70.−b, 74.25.Jb, 79.60.−i, 71.20.−b DOI: 10.1088/0256-307X/33/7/077402

Iron-based superconductors consist of various systems with distinct crystal structures and different optimal superconducting transition temperatures.[1−5] They are exemplified by four representative systems such as AFeAsO (A=Ce, Pr, Sm, etc.) known as the 1111 system, RFe$_2$As$_2$ (R=Ba, Ca, Sr, etc) known as the 122 system, MFeAs (M=Na and Li) known as the 111 system and FeSe known as the 11 system. These systems share the common FeAs/FeSe layers (Figs. 1(a) and 1(b)) that are believed to be the essential elements to dictate superconductivity. In most of the iron-based systems, the parent compounds are antiferromagnetic poor metals, and superconductivity is realized by suppressing the antiferromagnetic order through either chemical substitution or pressure applications. It is also found that the antiferromagnetic transition usually occurs either simultaneously with or slightly below a tetragonal-orthorhombic structural transition. The FeSe system is unique in that this parent compound exhibits a structural transition near 90 K, while does not show the long-range antiferromagnetic order and is already superconducting with a T_c around 9 K.[6−8] Recently, two distinct phases (N phase and S phase) are observed in the FeSe films grown on $SrTiO_3$ substrates where the N phase resembles the parent compounds of the bulk iron-based superconductors, while the S phase can show high temperature superconductivity with T_c as high as 65 K.[9−17] It has been found that for the parent compounds and underdoped samples, a nematic phase transition occurs at or above the structural/antiferromagnetic transition temperatures, which breaks the rotational symmetry while preserving the translational symmetry of lattice.[18−26] Understanding the origin of nematicity and its relation with superconductivity is essential in understanding the superconductivity mechanism of the iron-based superconductors.[27−36]

In this Letter, we report our comprehensive angle-resolved photoemission (ARPES) study on the electronic structure and nematicity in the parent compounds of the iron-based superconductors including CeFeAsO, $BaFe_2As_2$, NaFeAs, FeSe and undoped FeSe/$SrTiO_3$ films with 1, 2 and 20 layers. We found

*Supported by the National Natural Science Foundation of China under Grant Nos 11190022, 11334010 and 11534007, the National Basic Research Program of China under Grant No 2015CB921000, and the Strategic Priority Research Program (B) of Chinese Academy of Sciences under Grant No XDB07020300.

**Corresponding author. Email: XJZhou@iphy.ac.cn

© 2016 Chinese Physical Society and IOP Publishing Ltd

that, although the electronic structures near the Brillouin center Γ vary dramatically among different compounds, the electronic structures near the Brillouin zone corners (M points), including the Fermi surface, band structure and temperature dependence, are rather similar. The electronic structures near the zone corners are dominated by electronic nematicity that gives rise to a band splitting of the d_{xz} and d_{yz} bands below the nematic transition temperature. A clear relation is established between the d_{xz} and d_{yz} bands splitting and the onset temperature of nematicity. Our results will shed light on the origin of nematicity, its effect on the electronic structures, and its relation with superconductivity in the iron-based superconductors.

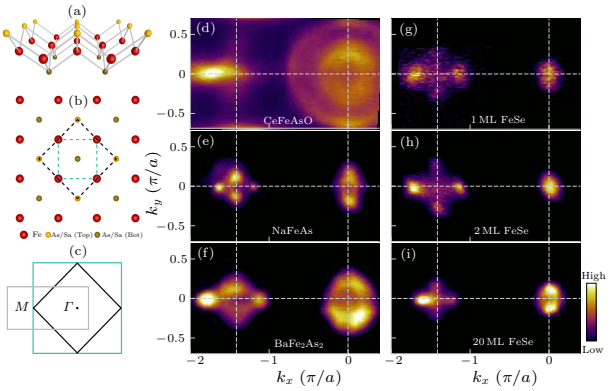

Fig. 1. Fermi surface mapping of some parent compounds of the iron-based superconductors and FeSe/SrTiO$_3$ thin films. (a) Three-dimensional view of the FeAs/FeSe layer in the iron-based compounds. (b) Top view of the FeAs/FeSe layer. (c) The corresponding Brillouin zones. The blue square corresponds to the Brillouin zone with one Fe in a unit cell while the black square represents the Brillouin zone with two irons in one unit cell that we generally adopt. Grey rectangle indicates the momentum space that is covered in our ARPES measurements. (d)–(i) Fermi surface mapping of CeFeAsO (d), NaFeAs (e), $BaFe_2As_2$ (f), 1 ML FeSe/SrTiO$_3$ film (g), 2 ML FeSe/SrTiO$_3$ film (h) and 20 ML FeSe/SrTiO$_3$ film (i) measured at $\sim$20 K.

The ARPES measurements are carried out on our photoemission system equipped with a Scienta R4000 electron energy analyzer and a Helium discharge lamp which gives a photon energy of $h\nu$ = 21.218 eV.[11,14,37–40] The light on the sample is partially polarized. The energy resolution was set at 10 meV and the angular resolution is $\sim$0.3°. The Fermi level is referenced by measuring on the Fermi edge of a clean polycrystalline gold that is electrically connected to the sample. The samples were measured in vacuum with a base pressure better than 5×10^{-11} Torr. We note that as FeSe/SrTiO$_3$ films may be doped with electrons by either vacuum annealing[11,14] or potassium deposition,[16,41,42] the single-layer (1 ML), double-layer (2 ML) and 20-layer (20 ML) FeSe/SrTiO$_3$ films we measured here all are undoped with their net doping close to zero.

Figure 1 shows the Fermi surfaces of CeFeAsO, NaFeAs, $BaFe_2As_2$ and FeSe/SrTiO$_3$ films (1 ML, 2 ML and 20 ML) at 20 K. The corresponding band structures across the Γ point and M point are shown in Figs. 2 and 3, respectively. Note that the electronic structure of CeFeAsO may be affected by polarized surface and surface state.[40,43] Overall, the Fermi surface of these compounds shows a dramatic difference near the Γ point. First, although there are hole-like Fermi surface sheets observed in CeFeAsO (Fig. 1(d)), NaFeAs (Fig. 1(e)), $BaFe_2As_2$ (Fig. 1(f)) and 20 ML FeSe/SrTiO$_3$ film (Fig. 1(i)) at the Γ point, there is no Fermi surface for 1 ML (Fig. 1(g)) and 2 ML (Fig. 1(h)) FeSe/SrTiO$_3$ films due to the fact that no band crosses Fermi level for these two samples (Fig. 2) (the signal at the Γ point for these two samples in Figs. 1(g) and 1(h) is due to residual spectral leakage). Secondly, the Fermi surface at the Γ point varies obviously in area and shape among CeFeAsO, NaFeAs, $BaFe_2As_2$ and 20 ML FeSe/SrTiO$_3$ films. On the other hand, the Fermi surface topology near the M point shows rather consistent patterns, i.e., four strong spots are observed around the M point. These strong spots are related to the formation of Dirac cone-like structures in these systems, similar to the case of $SrFe_2As_2$,[38] $BaFe_2As_2$[39,44] and multiple-layer FeSe/SrTiO$_3$ films[45] observed before.

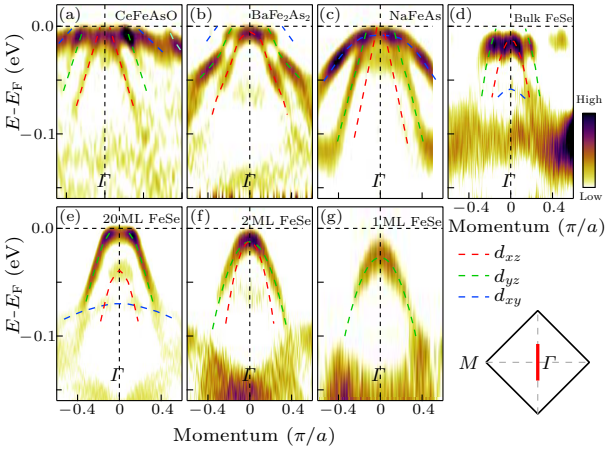

Fig. 2. Band structures of some parent compounds of the iron-based superconductors and FeSe/SrTiO$_3$ thin films near the Γ point measured at $\sim$20 K. (a) CeFeAsO, (b) $BaFe_2As_2$, (c) NaFeAs, (d) bulk FeSe, (e) 20 ML FeSe/SrTiO$_3$ film, (f) 2 ML FeSe/SrTiO$_3$ film and (g) 1 ML FeSe/SrTiO$_3$ film. The images are obtained by the second derivative of the original data with respect to energy. The orbital characters of the observed bands are labeled. The corresponding location of the momentum cut is shown as a red thick line in the bottom-right inset.

The band structures near the Γ point are rather different in these materials, as shown in Fig. 2. The observed bands can basically be assigned to d_{yz}, d_{xz} and d_{xy} orbitals except for the CeFeAsO case (Fig. 2(a)) where the outmost fourth band may come from the surface state.[40,43] However, the bands near

the Γ point are rather different in terms of the total number of bands observed and the number of bands crossing the Fermi level. In particular, although there are bands crossing the Fermi level in CeFeAsO, $BaFe_2As_2$, NaFeAs and 20 ML FeSe/$SrTiO_3$ films, no Fermi crossing is observed for 1 ML and 2 ML FeSe/$SrTiO_3$ films. The relative position of the observed bands varies strongly among different materials, especially for the bands from the d_{xy} orbital.

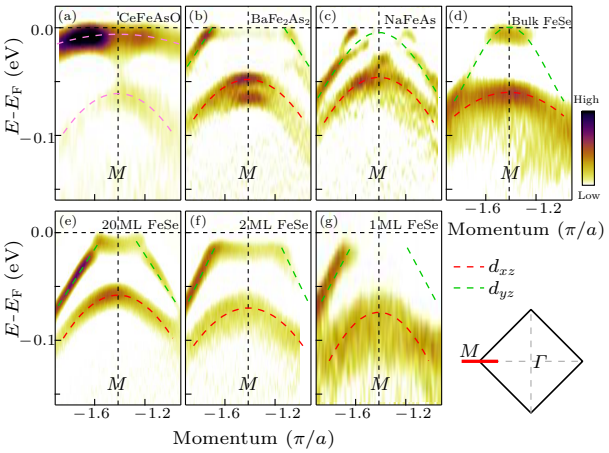

Fig. 3. Band structures of some parent compounds of the iron-based superconductors and FeSe/$SrTiO_3$ thin films near the M point measured at ∼20 K. (a) CeFeAsO, (b) $BaFe_2As_2$, (c) NaFeAs, (d) bulk FeSe, (e) 20 ML FeSe/$SrTiO_3$ film, (f) 2 ML FeSe/$SrTiO_3$ film and (g) 1 ML FeSe/$SrTiO_3$ film. The images are obtained by the second derivative of the original data with respect to energy. The orbital characters of the observed bands are labeled. The corresponding location of the momentum cut is shown as a red thick line in the bottom-right inset.

The band structures near the M point are rather similar for these materials measured, as shown in Fig. 3. Two main bands dominate the electronic structure near the M point: one hole-like band cross or near the Fermi level assigned to the d_{yz} orbital, and the other hole-like band that is at a high binding energy assigned to the d_{xz} orbital. The bright spots around the M point seen in Fig. 1 are caused by the d_{yz} band near the Fermi level. The band structure of CeFeAsO (Fig. 3(a)) is somehow different, probably it is affected by polar surface and surface state.[40,43] Some extra bands such as in NaFeAs (Fig. 3(c)) are due to band folding induced from the antiferromagnetic phase transition. Neglecting these extra complications, the band structure near the M point is rather consistent for FeAs- and FeSe-based materials, and for bulk materials and thin films.

Further measurements indicate that the electronic structures near the M point also exhibit a similar temperature dependence, as shown in Figs. 4(a)–4(f). Upon increasing temperature, the d_{yz} and d_{xz} bands near the M point gradually come close to each other. The d_{yz} band moves down while the d_{xz} band moves up. Eventually these two bands merge into a single band above a transition temperature. This transition temperature is close to the temperature of the structural transition in bulk parent compounds such as $BaFe_2As_2$, and NaFeAs and FeSe although it is not yet known whether there is a structural/magnetic transition in FeSe/$SrTiO_3$ films.

The electronic structure of the measured materials near the M point at low temperature is dramatically different from the band structure calculations. First, the overall band energy scale of the d_{xz}/d_{yz} and d_{xy} bands at the M point is much smaller than that from the band structure calculations.[46] Secondly, the band splitting of the d_{xz} and d_{yz} bands cannot be accounted for by the slight lattice constant difference between the a and b axes. Such a band splitting can be explained in terms of the band reconstruction from the electronic nematicity,[21,23,24] as schematically shown in Fig. 4(g). At high temperature above the nematic transition temperature $T_{\rm nem}$, the system is in a tetragonal phase with two electron Fermi surfaces located at the M point. At the $M1$ point, the d_{yz} band crosses the Fermi level and the d_{xz} band lies below the Fermi level. While at the $M2$ point, the d_{xz} band crosses the Fermi level and the d_{yz} band lies below the Fermi level. The d_{yz} and d_{xz} bands are degenerate at $M1$ and $M2$ points. Upon cooling down, the system undergoes a nematic transition and the rotational symmetry is broken, giving rise to a shifting of the d_{yz} band upwards and a shifting of the d_{xz} band downwards at both the $M1$ and $M2$ points. Due to the twinning effect in the sample we measured, the band structure we obtained at one M point is a combination of $M1$ and $M2$ points ($M1 + M2$ in Fig. 4(g)), which shows the split d_{yz} band and d_{xz} band below the Fermi level. Such a splitting increases with decreasing the temperature and can explain the observations quite well.

We define the temperature at which the d_{yz} and d_{xz} bands just start to emerge into each other as the nematic transition temperature. Figure 4(h) shows the temperature dependence of the splitting energy difference between the d_{yz} and d_{xz} bands at a designated momentum shown by the purple lines in Figs. 4(a)–4(f). One can see that they all show an decrease with increasing temperature and becomes zero above the nematic transition temperature $T_{\rm nem}$. Figure 4(i) summaries the splitting size between d_{yz} and d_{xz} bands at the M point as a function of the nematic transition temperature among various iron-based materials, with some data from previous works.[12,47] We can see that the nematic transition temperature and the band splitting between the d_{yz} and d_{xz} bands basically follow a linear relation.

The observation of common electronic features near the M point, and different electronic struc-

tures near the Γ point, in various parent compounds of the iron-based superconductors and undoped FeSe/$SrTiO_3$ films with different layers indicate that the M point electronic structure represents the generic electronic property of the parent compounds. The common electronic structure near the M point indicates that they have the same origin, i.e., they are dominated by the electronic nematicity. It has been under debate on the origin of nematicity whether it is due to spin fluctuation[27–31] or orbital fluctuation.[32–36] The absence of long-range antiferromagnetic order in bulk FeSe appears to contradict with the spin scenario although we note that magnetic signal in bulk FeSe is found to be strong[48] and spin fluctuation may act in different ways.[49–52] The dominant effect of nematicity on the M point electronic structure, and its weak effect on the Γ point, are not consistent with the on-site ferro-ordering picture which would expect to induce isotropic reconstruction along the Γ–M direction.[32] The origin of nematicity in the iron-based compounds and its relation with superconductivity are complex so that further investigations are needed.

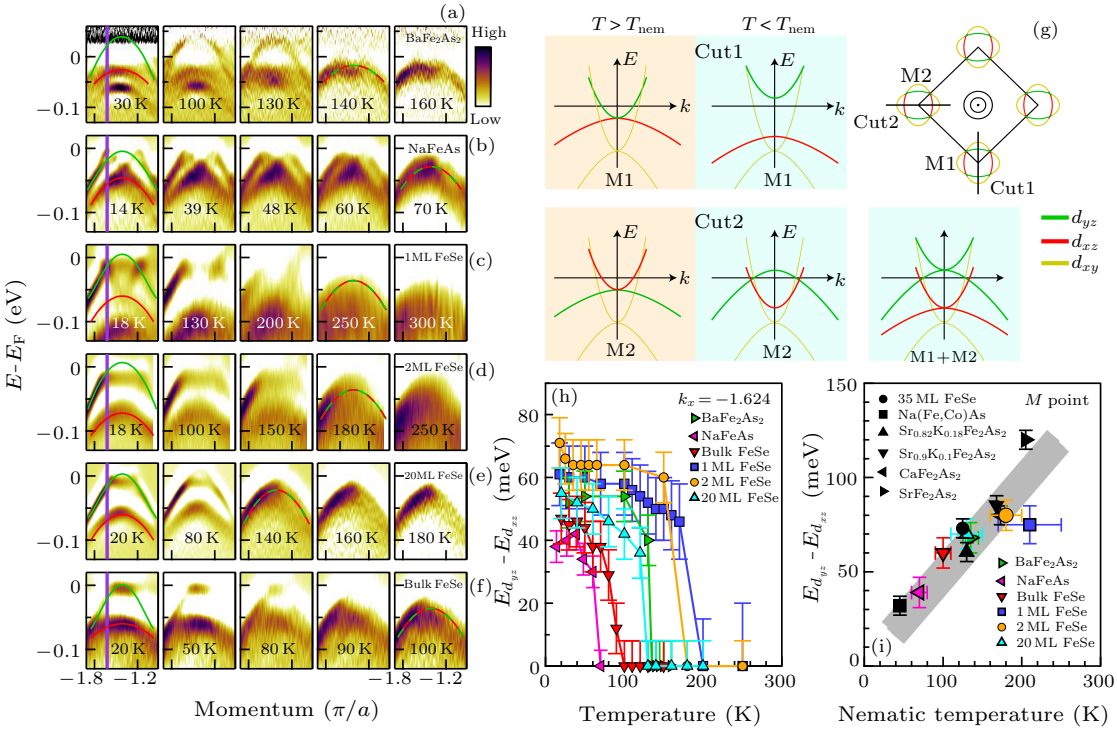

Fig. 4. Temperature dependence of the band structure near the M point. The location of the momentum cut is the same as shown in Fig. 3. (a)–(f) Temperature-dependent band structure measurements near the M points of $BaFe_2As_2$ (a), NaFeAs (b), 1 ML FeSe/$SrTiO_3$ film (c), 2 ML FeSe/$SrTiO_3$ film (d), 20 ML FeSe/$SrTiO_3$ film (e) and bulk FeSe (f). The d_{yz} and d_{xz} bands are labeled by green and red lines, respectively. They split at low temperatures and merge into a single band above the nematic transition temperature. (g) Schematic drawing of band structures near the M point above and below the nematic transition temperature. (h) Temperature dependence of the band splitting size between d_{yz} and d_{xz} bands at k_x near $-1.624\pi/a$ as indicated by the purple lines in (a)–(f). (i) Relation of the band splitting size between the d_{yz} and d_{xz} bands at the M point with the nematic transition temperature. Here the band splitting size refers to the energy difference at the M point at low temperature. The top of the d_{yz} band is estimated from fitting the measured d_{yz} band with a parabola. Data of the 35 ML FeSe/$SrTiO_3$ film is obtained from Ref. [47] and other data in black symbols are obtained from Ref. [12].

In summary, by carrying out comprehensive ARPES measurements on the parent compounds of the iron-based superconductors and undoped FeSe/$SrTiO_3$ films with various layers, we have extracted common electronic features near the M point, including the Fermi surface topology, band structure and temperature dependence. These observations indicate that the M point electronic structure represents the generic electronic property of the undoped parent compounds. Further, the M point electronic structure is dominated by the electronic nematicity that gives rise to band splitting of the d_{yz} and d_{xz} bands below the nematic transition temperature. There is a close relation between the band splitting magnitude and the nematic transition temperature. These results provide important information on studying the origin of electronic nematicity and its relation with superconductivity in the iron-based superconductors.

References

[1] Ishida K et al 2009 *J. Phys. Soc. Jpn.* **78** 062001
[2] Paglione J et al 2010 *Nat. Phys.* **6** 645
[3] Johnston D C 2010 *Adv. Phys.* **59** 803
[4] Stewart G R 2011 *Rev. Mod. Phys.* **83** 1589
[5] Wang F et al 2011 *Science* **332** 200
[6] Hsu F C et al 2008 *Proc. Natl. Acad. Sci. USA* **105** 14262
[7] McQueen T M et al 2009 *Phys. Rev. Lett.* **103** 057002
[8] Mizuguchi Y et al 2010 *Physica* C **470** S338
[9] Wang Q Y et al 2012 *Chin. Phys. Lett.* **29** 037402
[10] Liu D F et al 2012 *Nat. Commun.* **3** 931
[11] He S L et al 2013 *Nat. Mater.* **12** 605
[12] Tian S Y et al 2013 *Nat. Mater.* **12** 634
[13] Lee J J et al 2014 *Nature* **515** 245
[14] Liu X et al 2014 *Nat. Commun.* **5** 5047
[15] He J F et al 2014 *Proc. Natl. Acad. Sci. USA* **52** 18501
[16] Miyata Y et al 2015 *Nat. Mater.* **14** 775
[17] Liu X et al 2015 *J. Phys.: Condens. Matter* **27** 183201
[18] Chu J H et al 2010 *Science* **329** 824
[19] Tanatar M A et al 2010 *Phys. Rev.* B **81** 184508
[20] Chuang T M et al 2010 *Science* **327** 181
[21] Yi M et al 2011 *Proc. Natl. Acad. Sci. USA* **108** 6878
[22] Kasahara S et al 2012 *Nature* **486** 382
[23] Zhang Y et al 2012 *Phys. Rev.* B **85** 085121
[24] Yi M et al 2012 *New J. Phys.* **14** 073019
[25] Rosenthal E P et al 2014 *Nat. Phys.* **10** 225
[26] Nakayama K et al 2014 *Phys. Rev. Lett.* **113** 237001
[27] Fang C et al 2008 *Phys. Rev.* B **77** 224509
[28] Xu C et al 2008 *Phys. Rev.* B **78** 020501(R)
[29] Mazin I et al 2009 *Nat. Phys.* **5** 141
[30] Fernandes R M et al 2010 *Phys. Rev. Lett.* **105** 157003
[31] Fernandes R M et al 2014 *Nat. Phys.* **10** 97
[32] Lee C C et al 2009 *Phys. Rev. Lett.* **103** 267001
[33] Krüger F et al 2009 *Phys. Rev.* B **79** 054504
[34] Chen C C et al 2010 *Phys. Rev.* B **82** 100504(R)
[35] Kontani H et al 2011 *Phys. Rev.* B **84** 024528
[36] Lv W et al 2011 *Phys. Rev.* B **84** 174512
[37] Liu G D et al 2008 *Rev. Sci. Instrum.* **79** 023105
[38] Liu H Y et al 2008 *Phys. Rev.* B **78** 184514
[39] Liu G D et al 2009 *Phys. Rev.* B **80** 134519
[40] Liu H Y et al 2010 *Phys. Rev. Lett.* **105** 027001
[41] Wen C et al 2016 *Nat. Commun.* **7** 10840
[42] Ye Z R et al 2015 arXiv:1512.02526[cond-mat.supr-con]
[43] Liu C et al 2010 *Phys. Rev.* B **82** 075135
[44] Richard P et al 2010 *Phys. Rev. Lett.* **104** 137001
[45] Tan S Y et al 2016 *Phys. Rev.* B **93** 104513
[46] Singh D J et al 2008 *Phys. Rev. Lett.* **100** 237003
[47] Zhang Y et al 2015 arXiv:1503.01556[cond-mat.supr-con]
[48] Wang Q S et al 2015 *Nat. Mater.* **15** 159
[49] Chubukov A V et al 2015 *Phys. Rev.* B **91** 201105
[50] F Wang et al 2015 *Nat. Phys.* **11** 959
[51] Glasbrenner J K et al 2015 *Nat. Phys.* **11** 953
[52] Yu R et al 2015 *Phys. Rev. Lett.* **115** 116401